Article:

Fuchs, K., Medina Rivero, S., Weidlich, A. et al. (7 more authors) (2023) Dimerization of a reactive azaacene diradical: synthesis of a covalent azaacene cage. Angewandte Chemie International Edition. e202305712. ISSN 1433-7851

https://doi.org/10.1002/anie.202305712

Diradicals

Dimerization of a Reactive Azaacene Diradical: Synthesis of a Covalent Azaacene Cage

Kathleen Fuchs, Samara Medina Rivero, Anna Weidlich, Frank Rominger, Noel Israel,
Alexey A. Popov, Andreas Dreuw,* Jan Freudenberg,* Juan Casado,* and Uwe H. F. Bunz*

Abstract: Two series of regioisomeric dicyanomethylene substituted dithienodiazatetracenes with formal *para*- or *ortho*-quinodimethane subunits were synthesized and characterized. Whereas the *para*-isomers (*p*-n, diradical index $y_0 = 0.01$) are stable and isolable, the *ortho*-isomer ($y_0 = 0.98$) dimerizes into a covalent azaacene cage. Four elongated σ-CC bonds are formed and the former tri*iso*propylsilyl(TIPS)-ethynylene groups transformed into cumulene units. The azaacene cage dimer (*o*-1)$_2$ was characterized by X-ray single crystal structure analysis and temperature-dependent infrared (IR), electron paramagnetic resonance (EPR, solid-state), nuclear magnetic resonance (NMR) and ultraviolet-visible (UV/Vis) spectroscopies (solution) indicating reformation of *o*-1.

[*] K. Fuchs, Dr. F. Rominger, Dr. J. Freudenberg,
Prof. Dr. U. H. F. Bunz
Organisch-Chemisches Institut, Ruprecht-Karls-Universität Heidelberg
Im Neuenheimer Feld 270, 69120 Heidelberg (Germany)
E-mail: freudenberg@oci.uni-heidelberg.de
uwe.bunz@oci.uni-heidelberg.de

Dr. S. Medina Rivero, Prof. J. Casado
Department of Physical Chemistry, University of Málaga
Andalucia-Tech Campus de Teatinos s/n, 29071 Málaga (Spain)
E-mail: casado@uma.es

A. Weidlich, Prof. Dr. A. Dreuw
Interdisciplinary Center for Scientific Computing, Ruprecht-Karls-Universität Heidelberg
Im Neuenheimer Feld 205, 69120 Heidelberg (Germany)
E-mail: andreas.dreuw@iwr.uni-heidelberg.de

N. Israel, Dr. A. A. Popov
Center of Spectroelectrochemistry, Leibniz Institute for Solid State and Materials Research (IFW) Dresden
Helmholtzstraße 20, 01069 Dresden (Germany)

Dr. S. Medina Rivero
Department of Physics & Astronomy, University of Sheffield
S37RH Sheffield (UK)

Introduction

Dynamic covalent chemistry (DCC) exploits the reversible formation of chemical bonds by external soft stimuli.[1] It accesses metal-organic[2] and covalent-organic frameworks[2e,3] as well as macrocycles and cages[4] among others—the reversibility allows autonomous healing of defects to access thermodynamic sinks.[1d] DCC is not limited to condensation reactions as their most prominent representative[1c,2e]—σ-bond homolysis/radical dimerization[5] can also be utilized. For example, Seki et al. synthesized triarylamino-dicyanomethyl diradicals, which reversibly reacted to defined cyclic oligomers.[6] Closely related is the search for long (exceeding 1.54 Å[7]) and weak carbon-carbon σ-bonds. A number of reported cases are shown in Figure 1: Molecules **A**[8] and **B**[9] originate from intramolecular reactions while **C** and **D**[10] is formed by intermolecular dimerization of (intermediately generated) diradicals.

Diradicals are attractive for applications in organic electronics,[11] nonlinear optics[11b,12] and spintronics.[13] A great variety of carbon-based diradical(oid)s has been explored including zethrenes,[14] anthenes,[15] extended quinodimethanes,[16] bisphenalenyls,[17] the larger acenes,[18] indenofluorenes[19] and related diindenoacenes.[20] The diradical index y_0 characterizes the degree of open-shell character in a diradical. This value varies from 0 for closed-shell molecules to 1 in full open-shell structures.[21] Highly reactive diradicals polymerize forming inter-monomer σ-CC bonds, e.g. *p*-quinodimethane diradicals furnishing poly-*p*-xylylenes.[22] In the other extreme, stable diradicals are proaromatic structures that produce diradicals in the form of
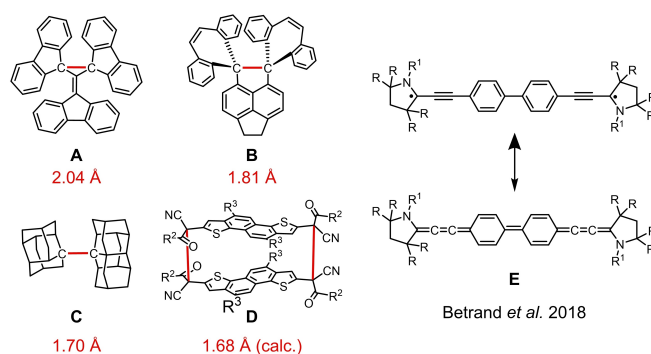

Figure 1. Chemical structures of molecules with long CC strained bonds **A**–**D**[8–10,26] together with Bertrand's acetylene-aromatic/cumulene-qui-noidal imine diradical **E**.[25]

quinoidal/aromatic resonant hybrids.[18d] Some of these aromatic diradicals with small to medium y_0 (≈ 0.1–0.6) values form long and therefore weak intermolecular σ-CC bonds.[10] Besides rearomatization of quinoids, the cumulenic to acetylenic transformation in long 1D carbon materials (i.e., carbyne)[23] has been long envisaged to stabilize diradicals by Jahn–Teller distortion, a situation still standing as a theoretical prediction.[24] Though the acetylene/cu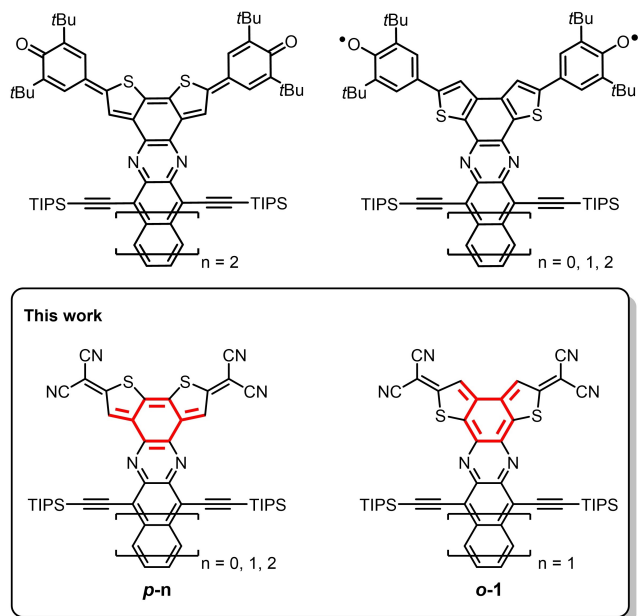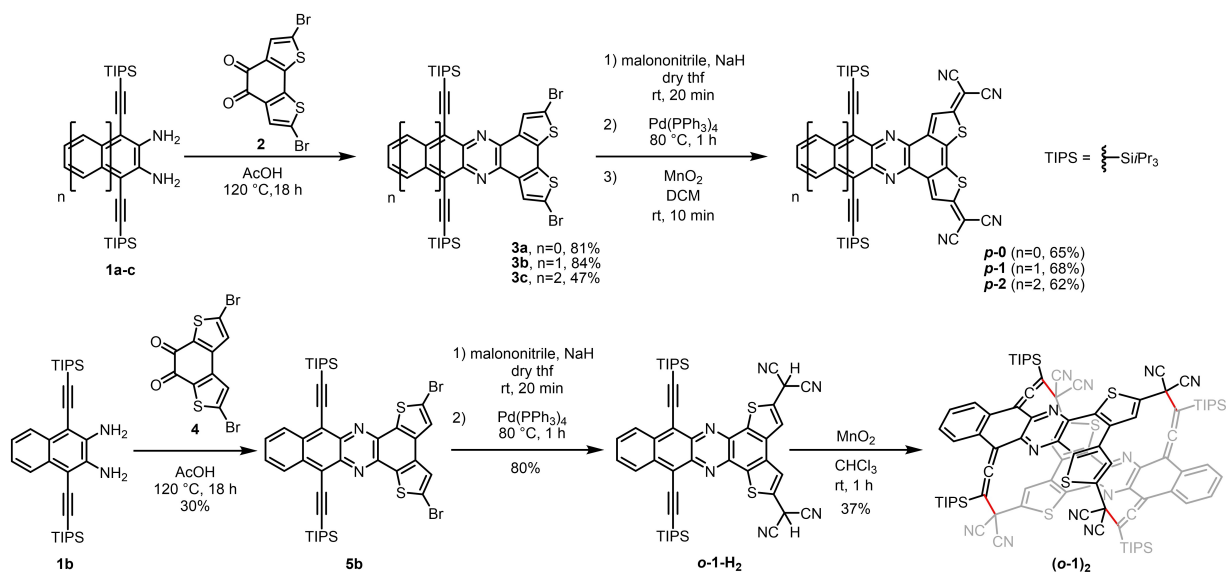mulene resonant hybrids seem insufficient, a new strategy by mixing them with aromatic/quinoidal forms can result in an alternative for the design of new diradicals. Bertrand et al. demonstrated that in the aromatic-acetylenic structure the diradical prevails over the full bonding quinoidal-cumulene form (**E**, Figure 1).[25]

Recently, some of us reported isomeric azaacene-extended phenoxylbithiophenequinoidals/radicals (Figure 2, top), in which the relative orientation of the sulfur atoms determines the diradical character.[18d] The problem can be re-formulated as the impact of *para-* vs. *ortho-*conjugation between the two moieties in the isomers. In this work, we transition to carbon-based diradicals by preparing dicyanomethylene substituted benzodithienophenazines (Figure 2, bottom *p-n* and *o-1*). Cross-conjugation of the *para-*quinoidal segment to the acene makes the systems electronically inert (closed-shell). The *ortho-*isomer however exhibits increased diradical character and intermolecularly dimerizes under formation of four long (≈ 1.6 Å) σ-CC bonds overall reverting the aromatic-acetylene monomer structure into a quinoidal-cumulene form in the cage dimer. This aromatic/acetylene to quinoidal/cumulene evolution transcends the chemical discipline and has been recently appointed as the main motif for the appearance of metallic edge states in topological insulators based on acene-acetylene polymers.[27]

Figure 2. Top: Previously reported phenoxyl-based azaacene quinoids/diradicals.[18d] Bottom: Chemical structures of the studied compounds herein. *p-n* and *o-1* include *para-* and *ortho-*xylylene substructures between the tetracyanated, quinoidal bithiophene segment (marked in red). The quinoidal resonance forms are depicted.

Results and Discussion

Scheme 1 shows the synthetic approach towards *p-n* and *o-1* by condensation of an aromatic diamine **1a–c** with the *ortho-*quinone **2** or **4** furnishing dibromides **3a–c** or **5b**. **3a–c** were reacted with malononitrile in a Pd-catalyzed cross-coupling. Manganese(IV) oxide oxidation furnished the series *p-n* ($n = 0$–2). Similarly, the synthesis of isomeric *o-1* was attempted, but it was too unstable for isolation. Instead

Scheme 1. Synthesis of quinoidal *p-n* (top) and of dimer (*o-1*)$_2$ (bottom, new bonds highlighted in red).

the dimerized compound $(o\text{-}1)_2$ was obtained as a yellow precipitate from the reaction mixture.

The absorption spectra of *p*-n (Figure 3b) are characterized by three groups of electronic bands. The two vibronically spaced bands at 590/577 nm in *p*-0, 588/551 nm in *p*-1 and 590/550 nm in *p*-2 are typical of the tetracyano bithienoquinoidal cores and independent of the size of the azaacene. A second group of bands appears at 295/377 nm in *p*-0, 321/405 nm in *p*-1, and 336/442 nm in *p*-2, assigned to the azaacene core. Their peak energy maxima vary with the azaacene's size in line with the increment of this π-conjugated core, as do the bands responsible for the more red-shifted absorption onsets reaching into the infrared for the longest congener *p*-2. These weak near infrared (NIR) bands correspond to the transition of the highest occupied molecule orbital (HOMO) to the lowest unoccupied molecule orbital (LUMO) (see Figure S10 and Table S1 for time-dependent density functional theory (TDDFT) calculations and assignments of the other bands) which move electron density within the azaacenylene part in agreement with their acene size dependence. Further, their small absorbance and broad shapes might arise from the pseudo-disjoint character of these orbitals (i.e., atoms with maximal electron density in the HOMO disclose minimal electron density in the LUMO+1, Figure S11). Hence, in these *para*-substituted derivatives the former set evolves independently from the latter two, a typical situation for cross-conjugated species.

A similar situation is observed in the cyclic voltammograms (vs. the ferrocene/ferrocenium redox couple) of the three *para*-compounds (Figure S18, Table S2). Two sets of two reduction events are observed for each species—the first set is attributed to the tetracyanobithiophene core and occurs at similar potentials in the three compounds whereas the second set arises from the reduction of the azaacene moiety—as expected, these electron affinities decrease with increasing length of the azaacene. Exemplarily, *p*-1 is reduced to its monoanion (−0.28 V) and dianion (−0.72 V) at relatively low potentials, whereas reduction to the radical trianion and to the tetraanion occurs at −1.64 V and −2.33 V.
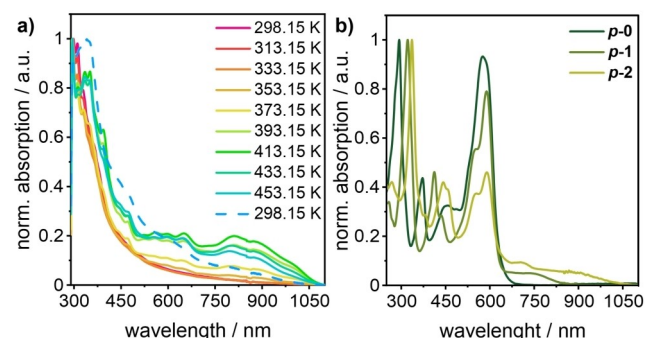
The electronic absorption and infrared spectra of the two first reduced species of the three *p*-n compounds have been obtained spectroelectrochemically (see Figure S5–S7 and Figure S15–S17).

The three IR and UV/Vis-NIR spectra of the three anions and dianions are essentially identical in accordance with cross-conjugation disruption of the electronic communication in between the *para*-quinoidal and azaacene paths that makes the first and second reduced species to be unaffected by the length of the azaacene. Single crystals of *p*-n were grown from diffusion of methanol into chloroform solution and measured at 200 K (X-ray structure of *p*-2, Figure 4a). Here the measured bond length alternation along the tetracyanated bithiophene segment (see Figure S3) undeniably set the quinoidal resonance form as the dominant one.

The silence in the EPR fits the negligible calculated diradical-character of $y_0 = 0.01$—in contrast to the phenoxy analogues with strong EPR signals and medium diradical-character $y_0 = 0.2$–0.3.

This preamble with the intramolecular "cross-conjugated" electronic properties of the studied compounds prepares the scene to afford the unexpected evolution of the *o*-1 diradical by intermolecular dimerization, probably diffusion controlled into $(o\text{-}1)_2$, which is investigated by single crystal X-ray crystallography (see Figure 4b–e). Intermediately generated diradical *o*-1 dimerized to cage-like $(o\text{-}1)_2$ with no internal, accessible cavity, similar to phanes[29], in a head-to-tail fashion (see Figure 4f and Figure S25). The

Figure 3. a) Variable temperature UV/Vis-NIR electronic absorption spectra of the $(o\text{-}1)_2$ in *o*-dichlorobenzene under argon atmosphere from room temperature (rt; red line) to 180 °C (green line) and after allowing to cool to room temperature (blue dotted line). b) Electronic absorption spectra of the *p*-n compounds in dichloromethane at room temperature.
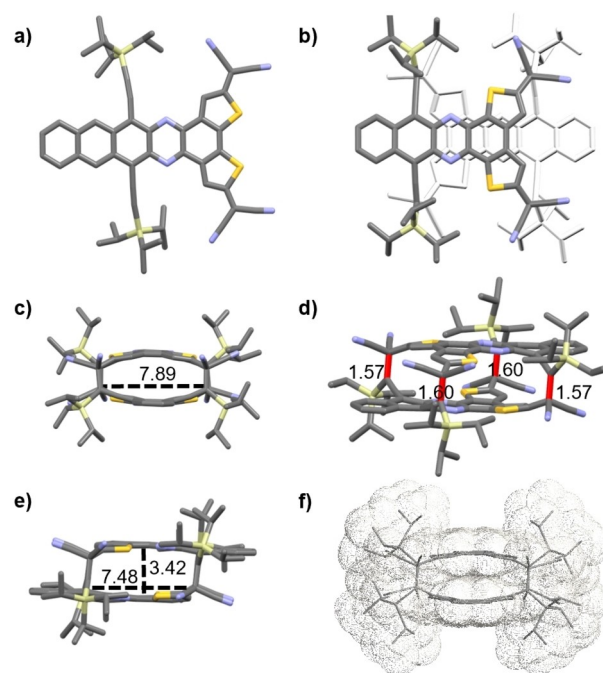
Figure 4. X-ray single crystal structure (200 K) of *p*-2 (a) and $(o\text{-}1)_2$ (b) as capped sticks. b)–e) Dimer $(o\text{-}1)_2$ from different perspectives including molecular dimensions in Å and σ-CC bond lengths. f) Illustration of the solvent accessible surface area with $r = 0.6$ Å of $(o\text{-}1)_2$ as capped sticks and wire mesh model. The elongated C–C bonds are highlighted in red (d). H-atoms were omitted for clarity.[28]

four new, symmetry equivalent bonds are 1.6 Å/1.57 Å long and located at the position of the fusion of the two molecules of *o*-1 (Figure 4d); π–π distances of the slightly curved aromatic backbones do not exceed 3.43 Å. The thiophene rings are fully aromatic supporting the diradical *o*-1 as putative intermediate. Diradicals with $y_0 \approx 1$ (i.e., *o*-1) can be rather stable, such as the case of their previously reported phenoxyl analogues. The formation of four-fold σ-CC bonded dimers is unprecedented in the sense that dimers arising from reactive diradicals are typically connected by two σ-CC bonds.[5a] Another feature of this solid-state cage is the formation of cumulene bonds formed at the expenses of the acetylene triple bonds of the lateral TIPS groups (previously considered only as spectating, solubilizing groups). A similar arrangement was recently observed by Kubo et al. with trimethylsilyl-ethynylene groups.[30] The relative stability of cumulene versus acetylene is of relevance as most of the known structures preferentially stabilize the acetylene mode. Here, in our dimer (*o*-1)$_2$, cumulenic structures are enforced around two quinoidal benzenes of the azaacene, a combination that in most of the known cases is unfavorable: It is locked into place by the superior stability provided by the four long strained σ-CC bonds as well as the generation of four aromatic Clar sextets per monomeric subunit (see Figure S2; in comparison, a conventional, alkyne-based head-to-head dimer would only exhibit three).

How stable is the cage and is dimerization reversible? The dimer has been spectroscopically characterized in the solid-state and in solution. In a *o*-dichlorobenzene solution, the UV/Vis spectrum of (*o*-1)$_2$ is characterized by an intense band at 310/328 nm which is plainly blue-shifted compared with the bands of the *para*-substituted *p*-1 (Figure 3). Heating this solution under argon atmosphere produces a drastic change with new bands appearing at 556, 597, 648 and 805 nm with an absorbance tail up to 1100 nm (see Figure 3a). This is typical of neutral open-shell diradicals, such as predicted and calculated for monomeric *o-1* (Figure S9). Notice here the different nature (disjoint-vs-diradical) of the origin of the weak NIR bands of *p*-1 and of *o*-1.

Heating the solution in air produces a change of the spectra, too. New bands appear at 528 nm, 619 and 687 nm with a tail up to 850 nm (Figure S8). Cooling back the solution to room temperature does not recover the original spectrum and an intermediate situation between the freshly prepared dimer and that upon heating is found. The variable temperature (VT) NMR study in tetrachloroethane-d_2 (Figure S19, S20) of (*o*-1)$_2$ shows that from a temperature of 373 K onwards, new signals appear in the aromatic region of the NMR spectrum. After cooling, these signals remain (see Figure S21, S22) indicating an irreversible process—the formation of o-1-H$_2$ as one of the degradation products further supports the cleavage of the σ-CC bonds. Mass analysis of the previously heated sample under nitrogen atmosphere indicates that the *decay products* are different dimers, trimers and, possibly, higher oligomers (see Figure S24).

In the solid-state dimer (*o*-1)$_2$, variable temperature fourier-transform infrared spectroscopy (VT-FT-IR) has

been carried out and is displayed in Figure 5a and Figure S12 (full spectra). The starting spectrum of (*o*-1)$_2$ at 298 K has a strong infrared band at 1907 cm^{-1} which is assigned to the stretching vibration of the cumulene CCC moiety; whereas at 2254 cm^{-1} a weak band is observed that arises from the CN stretching mode ($\approx$2260 cm^{-1} in a fully unconjugated cyano group as that of acetonitrile) and reflecting the observed pyramidalization (sp^3 character) of the methylene carbon atoms in the dimer (see Figure S13 and Figure S14 for the assignment of these vibrational modes). Upon heating, the 2254/1907 cm^{-1} pair of bands progressively disappears giving way to the increase of an infrared absorption at 2201 cm^{-1} due to the CN stretching mode of the cyano groups. This cyano band is accompanied by a low absorbance infrared feature at 2125 cm^{-1} which can be assigned to the CC stretching mode of the acetylene groups. The shift of the cyano bands 2254→2201 cm^{-1} on heating indicates the recovery of the sp^2 character of the methylene carbon upon planarization of the dicyano moiety with the bithiophene in the dissociated monomer product. The 2201 cm^{-1} band is typical for tetracyano thienoquinoidal diradicals.[31] By cooling back to 298 K, the IR spectrum of the starting material does not recover in line with the increasing inter-monomer disorder at high temperature that prevents the suitable reorientation/alignment of the radicals between monomers to re-bonding, further supporting the irreversibility of the thermal cycle and in agreement with the mass and NMR results in the heated solution. This FT-IR study documents a neat conversion of the cumulene-quinoidal dimer into an acetylene-aromatic structure upon
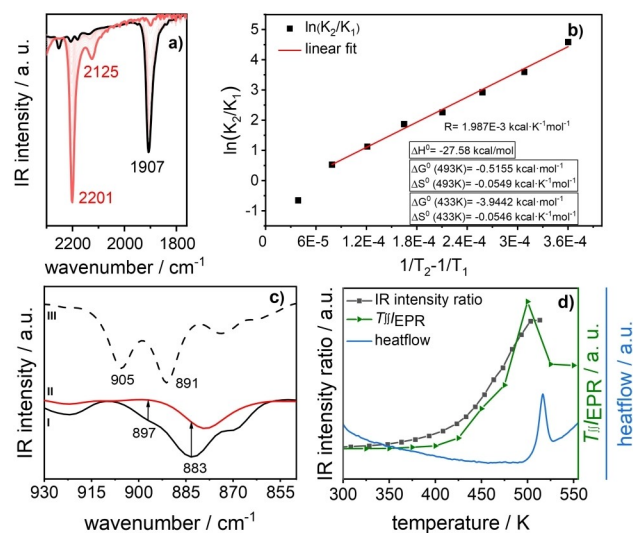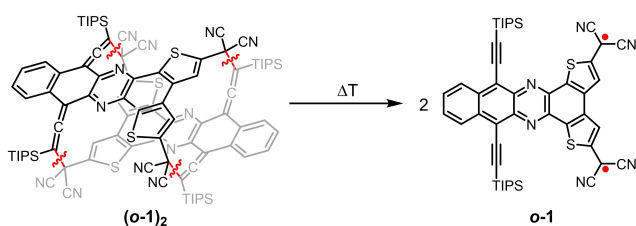

Figure 5. a) FT-IR spectra of (*o*-1)$_2$ in solid-state upon heating from room temperature (black line) to 240°C (red line). b) Van't Hoff fitting for the dimerization process in the solid-state from the absorbances of the 2201 and 1907 (bands) with universal gas constant R. c) Theoretical infrared spectrum at the B3LYP/6-31G** level of the dimer from the crystalline structures (**III**), the experimental IR spectra at room temperature (**I**) and upon heating to 240°C (**II**). d) Comparison of the intensity ratio of the increasing CN band at 2201 cm^{-1}, DSC plot (N$_2$) and $T \int\int I_{EPR}$ vs. temperature.

heating in agreement with the rupture of the long weak and strained σ-CC bonds of the dimer by thermal excitation.

The resolution of the neat interconversion of the cumulene (in the dimer) and of the cyano stretching modes (in the diradical monomers) as a function of temperature allows to calculate the monomer/dimer population ratio at each temperature for the dimer breaking reaction (dedimerization, see Scheme 2) which upon adjustment to a van't Hoff's plot (Figure 5b) leads to the thermodynamic and energetic landscape of the reaction. This van't Hoff modelling is qualitative as the reaction is occurring in the solid-state but it provides a variation of standard enthalpy for the solid-state reaction of -27.58 kcal mol^{-1} which should be in the order of magnitude of the real involved energies (see below the quantum chemical description of the reaction process). Nonetheless, this data reveals the formation of $(o\text{-}1)_2$ is exothermically driven with significant stabilization energy upon generation of four CC bonds. The theoretical infrared spectrum of the dimer structure of $(o\text{-}1)_2$ has been calculated at the B3LYP/6-31G** level (see Figure 5c and Figure S13c (full spectrum)) where the vibrational modes of the theoretical bands at 905 cm^{-1} (experimentally at 897 cm^{-1}) and at 891 cm^{-1} (experimentally at 883 cm^{-1}) clearly contain the CC stretches of the four weak long σ-CC bonds such as shown by its associated eigenvector in Figure S14. These two experimental infrared bands disappear upon heating in consonance with the rupture of the connecting bonds in the dimer. Reported IR vibrational studies of long strained σ-CC bonds between π-conjugated

organic molecules[32] document similar wavenumber values for the infrared bands associated with the stretching vibrational modes of the long strain CC bonds.

Differential scanning calorimetry (DSC) was carried out under nitrogen and ambient atmosphere (Figure 5d and Figure S23). There is one main exothermic signal in the heatflow at 500–525 K (integration furnishes 28.8 kcal mol^{-1}; in the order of magnitude of the real involved energies).

Complementary study of the thermal evolution of $(o\text{-}1)_2$ was performed by EPR spectroscopy (Figure 6). The pristine sample showed only a weak EPR signal at room temperature, in agreement with the singlet state suggested for the dimer. During heating, the EPR signal showed only modest increase while the temperature remained below 400 K, but exhibited a fast intensity increase above 400 K and all the way up to 500 K. After that a strong decline in the intensity is observed. Upon cooling the sample back to room temperature, the EPR intensity remained almost intact, indicating the dimer rupture is irreversible. This temperature onset of the fast dimer decomposition as well as its irreversibility correspond well to the observation of IR and UV/Vis spectroscopic studies. The comparison of the DSC signal with the intensity ratio of the appearing cyano-band at 2201 cm^{-1} (marks formation of $o\text{-}1$) from the FT-IR and the course of the EPR signal (Figure 5d) suggests that the maximum amount of free diradical $o\text{-}1$ is reached at ≈ 500 K and after that decomposition starts.

Quantum chemical calculations of the frontier molecular orbitals of the $p\text{-}1$ and $o\text{-}1$ were carried out (Figure 7, highest occupied Mos dissected in terms of the p$_z$ atomic coefficients). Π–conjugation and orbital overlap between the α-carbons of the two thiophenes of $p\text{-}1$ are strong, facilitating π-electron delocalization and full bonding between the terminal dicyanomethylenes. The largest p$_z$ coefficients in the α-carbons of the thiophenes result in an electronic pattern resembling that of a cross conjugated trimethylenemethane (TMM). Π-Electron delocalization by the β-carbons between thiophenes in $p\text{-}1$ is impeded by the aromatic character of the annelated pyrazine ring. Overall, the strong conjugation and π-bonding between the two thiophenes force these systems into closed-shell structures with electronic segregation between the constituting units. For the $p\text{-}n$ series, negligible values for y_0 are obtained ($y_0 = 0.01$), contrasting with the partial open-shell character ($y_0 = 0.2$–0.3) of the analogous phenoxyl compounds

Scheme 2. Cleavage of the azaacene cage $(o\text{-}1)_2$ into the proposed intermediate $(o\text{-}1)$.
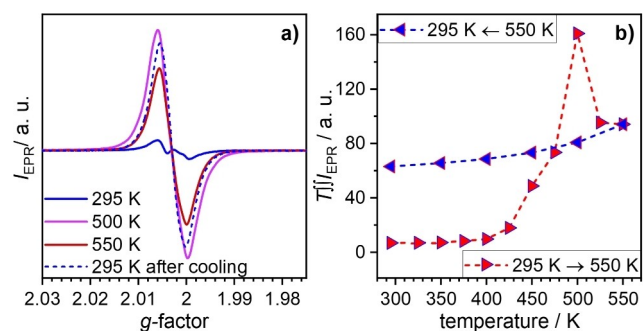

Figure 6. a) EPR spectra of powder $(o\text{-}1)_2$ measured at 295 K, after heating the sample to 550 K, and after cooling back to 295 K; b) the product of temperature and doubly-integrated EPR intensity ($T\iint I_{EPR}$) measured during heating the sample from 295 K to 550 K and cooling back to 295 K.
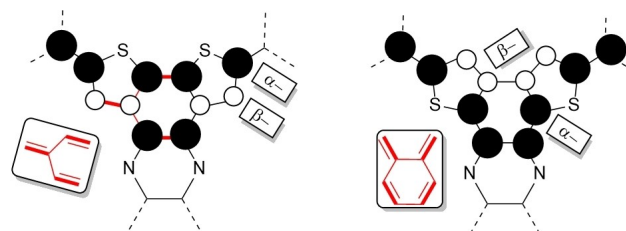

Figure 7. Orbital pattern dictating the main features of the electronic structure of the *para-* (left) and *ortho*-conjugated (right) compounds. In red, the TMM and ortho-benzene units are highlighted.

(Figure 2) due to the energy stabilization by phenoxyl aromatization.

Isomerization in *o*-1 drives the largest p_z-p_z overlap between thiophenes by their α-positions *through the connecting pyrazine of the azaacene*. This orbital pattern reveals a disruption of the aromaticity of the pyrazine (in comparison to *p*-1) in favor of an *ortho*-conjugation pattern in the terminal benzene ring of the azaacene and the thiophenes. The *ortho*-conjugation favors synergistic interaction between the bithiophene and the azaacene inherently resulting in a diradical (by the formation of an aromatic azaacene) with $y_0 = 0.98$ for *o*-1 at the UCAM-B3LYP/def-svp level of theory.

In accordance with the respective diradical character, spin-flip time-dependent density functional theory (SF-TDDFT) calculations show that *o*-1 has an open-shell singlet ground-state with an energy gap to the $m_s = 0$ triplet state of 0.01 eV (0.23 kcal mol⁻¹), while *p*-1 has a closed-shell singlet
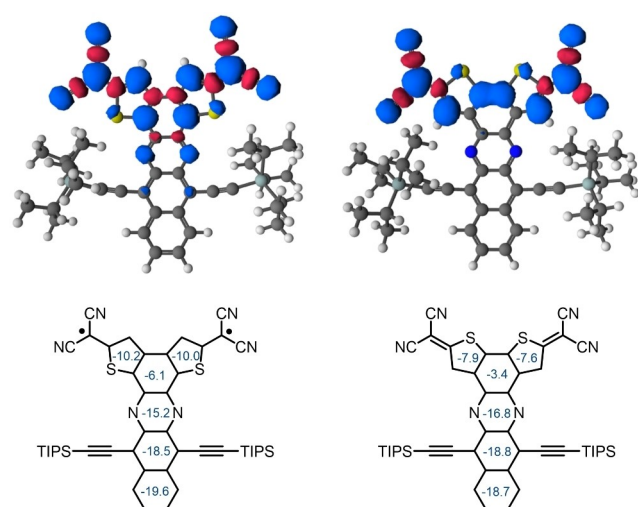
ground state with a singlet-triplet gap of 1.3 eV (29.98 kcal mol⁻¹). Spin densities of the triplet states are shown in Figure 8. In *o*-1 the density extends over the quinoidal system into the annulated acene. In *p*-1 it is confined to the former, since the acene backbone is a separate aromatic system. NICS(1.7)$_{zz}$ values were calculated for *o*-1 in the triplet state and for *p*-1 in the singlet state. The open-shell diradical ground state of *o*-1 results in larger aromatic NICS values as compared to the closed-shell quinoidal ground state of *p*-1.

To gain insight into the formation of the $(o\text{-}1)_2$ dimer from *o*-1, possible reaction pathways were investigated computationally using the GFN2-xTB method[33] (Figure 9). The results suggest the formation of the head-to-tail-π-dimer as a possible first reaction step, with an energy gain of −26.52 kcal mol⁻¹. Subsequently, the reaction could proceed via the head-to-tail-2σ intermediate (−63.38 kcal mol⁻¹), which outlines for the consecutive formation of two sets of two σ-bonds as opposed to a concerted mechanism forming four σ-bonds simultaneously. The formation of the head-to-head-2σ-dimer is disfavored compared to the cage by 63.54 kcal mol⁻¹. Focusing on the last reaction step, a slightly lower energy barrier for the stepwise formation of the last two σ-bonds by 3.9 kcal mol⁻¹ was observed in comparison to the simultaneous formation. The investigation did however not yield any intermediate structures containing one (or three) σ-bond(s). Based on these results, it is reasonable to consider the consecutive formation of two sets of two σ-bonds via the head-to-tail-2σ-dimer as a plausible reaction mechanism (see Supporting Information for detailed description of mechanistical investigation).

Figure 8. Spin-densities and NICS(1.7)zz values for *o*-1 and *p*-1 in the triplet state. NICS(1.7)$_{zz}$ value for *p*-1 were calculated in the singlet state.
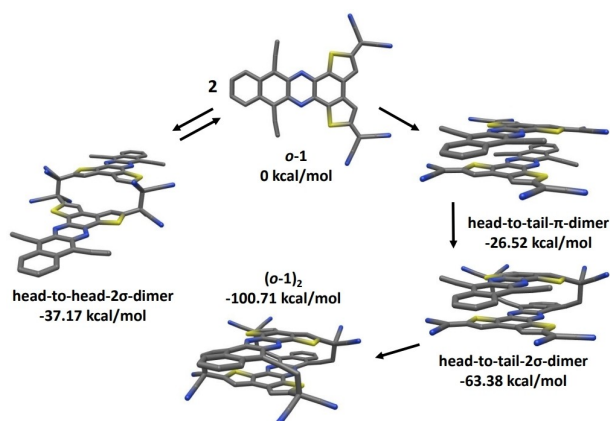
Conclusion

We successfully prepared regioisomeric dicyanomethylene substituted dithienodiazatetracenes with lateral "solubilizing" TIPS-ethynylene groups. The *para*-isomers (*p*-n) are stable, quinoidal, closed-shell species. The *ortho*-isomer *o*-1 is a diradical open-shell species/intermediate which surprisingly dimerizes to a covalent azaacene cage cumulenizing the former TIPS-ethynylene groups revealing their active electronic role far from being just innocent solubilizers. The formation of four σ-CC is uncommon for diradical dimers, as most are typically built with just two σ-CC bonds. $(o\text{-}1)_2$ is stable under ambient conditions—but variable temperature experiments of IR, NMR, UV/Vis and EPR suggest the reformation of the diradical *o*-1 and subsequent decomposition at elevated temperatures. We predict a stepwise, reversible dimerization process induced by the energy gain through head-to-tail π-dimerization. Control over the mode of dimerization (cage formation vs. head-to-head dimer) should be achievable through variation of the silyl groups as well as the functional groups adjacent to the radical center—this is underway in our laboratories.

Figure 9. Structures and relative free energies of *o*-1, $(o\text{-}1)_2$ and possible reaction intermediates of the dimerization process (obtained using the GFN2-xTB method). TIPS-groups and H-atoms were omitted for clarity.

Conflict of Interest

The authors declare no conflict of interest.

Data Availability Statement

Data related to this article from Heidelberg University are available via heiDATA (institutional research data repository of Heidelberg University) under the following DOI: https://doi.org/10.11588/data/QO118B.

Keywords: Azaacene Cage · Cumulene · Cyclization · Diradical · σ-Dimerization

[1] a) J.-M. Lehn, *Chem. Soc. Rev.* **2007**, *36*, 151–160; b) P. T. Corbett, J. Leclaire, L. Vial, K. R. West, J.-L. Wietor, J. K. M. Sanders, S. Otto, *Chem. Rev.* **2006**, *106*, 3652–3711; c) Y. Jin, C. Yu, R. J. Denman, W. Zhang, *Chem. Soc. Rev.* **2013**, *42*, 6634–6654; d) S. J. Rowan, S. J. Cantrill, G. R. Cousins, J. K. Sanders, J. F. Stoddart, *Angew. Chem. Int. Ed.* **2002**, *41*, 898–952.

[2] a) J. J. Perry IV, J. A. Perman, M. J. Zaworotko, *Chem. Soc. Rev.* **2009**, *38*, 1400–1417; b) D. J. Tranchemontagne, J. L. Mendoza-Cortés, M. O'Keeffe, O. M. Yaghi, *Chem. Soc. Rev.* **2009**, *38*, 1257–1283; c) M. O'Keeffe, *Chem. Soc. Rev.* **2009**, *38*, 1215–1217; d) J. R. Long, O. M. Yaghi, *Chem. Soc. Rev.* **2009**, *38*, 1213–1214; e) J. Hu, S. K. Gupta, J. Ozdemir, H. Beyzavi, *ACS Appl. Nano Mater.* **2020**, *3*, 6239–6269.

[3] a) S.-Y. Ding, W. Wang, *Chem. Soc. Rev.* **2013**, *42*, 548–568; b) X. Feng, X. Ding, D. Jiang, *Chem. Soc. Rev.* **2012**, *41*, 6010–6022; c) A. P. Côté, A. I. Benin, N. W. Ockwig, M. O'Keeffe, A. J. Matzger, O. M. Yaghi, *Science* **2005**, *310*, 1166–1170.

[4] a) A. Granzhan, C. Schouwey, T. Riis-Johannessen, R. Scopelliti, K. Severin, *J. Am. Chem. Soc.* **2011**, *133*, 7106–7115; b) S. Huang, Z. Lei, Y. Jin, W. Zhang, *Chem. Sci.* **2021**, *12*, 9591–9606; c) T. Hasell, A. I. Cooper, *Nat. Rev. Mater.* **2016**, *1*, 16053; d) M. Mastalerz, *Angew. Chem. Int. Ed.* **2010**, *49*, 5042–5053; e) T. H. G. Schick, F. Rominger, M. Mastalerz, *J. Org. Chem.* **2020**, *85*, 13757–13771.

[5] a) D. Sakamaki, S. Ghosh, S. Seki, *Mater. Chem. Front.* **2019**, *3*, 2270–2282; b) M. Frenette, C. Aliaga, E. Font-Sanchis, J. C. Scaiano, *Org. Lett.* **2004**, *6*, 2579–2582; c) H. Hartzler, *J. Org. Chem.* **1966**, *31*, 2654–2658.

[6] T. Kobashi, D. Sakamaki, S. Seki, *Angew. Chem. Int. Ed.* **2016**, *55*, 8634–8638.

[7] a) J. J. Novoa, P. Lafuente, R. E. Del Sesto, J. S. Miller, *Angew. Chem. Int. Ed.* **2001**, *40*, 2540–2545; b) J. P. Paolini, *J. Comput. Chem.* **1990**, *11*, 1160–1163.

[8] T. Kubo, Y. Suga, D. Hashizume, H. Suzuki, T. Miyamoto, H. Okamoto, R. Kishi, M. Nakano, *J. Am. Chem. Soc.* **2021**, *143*, 14360–14366.

[9] a) Y. Ishigaki, T. Shimajiri, T. Takeda, R. Katoono, T. Suzuki, *Chem* **2018**, *4*, 795–806; b) T. Takeda, H. Kawai, R. Herges, E. Mucke, Y. Sawai, K. Murakoshi, K. Fujiwara, T. Suzuki, *Tetrahedron Lett.* **2009**, *50*, 3693–3697.

[10] J. L. Zafra, L. Qiu, N. Yanai, T. Mori, M. Nakano, M. P. Alvarez, J. T. L. Navarrete, C. J. Gómez-García, M. Kertesz, K. Takimiya, *Angew. Chem. Int. Ed.* **2016**, *55*, 14563–14568.

[11] a) H. Koike, M. Chikamatsu, R. Azumi, J. y. Tsutsumi, K. Ogawa, W. Yamane, T. Nishiuchi, T. Kubo, T. Hasegawa, K. Kanai, *Adv. Funct. Mater.* **2016**, *26*, 277–283; b) X. Hu, W. Wang, D. Wang, Y. Zheng, *J. Mater. Chem. C* **2018**, *6*, 11232–11242.

[12] a) M. Nakano, B. Champagne, *J. Phys. Chem. Lett.* **2015**, *6*, 3236–3256; b) M. Nakano, R. Kishi, S. Ohta, H. Takahashi, T. Kubo, K. Kamada, K. Ohta, E. Botek, B. Champagne, *Phys. Rev. Lett.* **2007**, *99*, 033001; c) M. Nakano, R. Kishi, T. Nitta, T. Kubo, K. Nakasuji, K. Kamada, K. Ohta, B. Champagne, E. Botek, K. Yamaguchi, *J. Phys. Chem. A* **2005**, *109*, 885–891.

[13] Y. Morita, S. Suzuki, K. Sato, T. Takui, *Nat. Chem.* **2011**, *3*, 197–204.

[14] a) Y. Li, W.-K. Heng, B. S. Lee, N. Aratani, J. L. Zafra, N. Bao, R. Lee, Y. M. Sung, Z. Sun, K.-W. Huang, *J. Am. Chem. Soc.* **2012**, *134*, 14913–14922; b) W. Zeng, Z. Sun, T. S. Herng, T. P. Gonçalves, T. Y. Gopalakrishna, K. W. Huang, J. Ding, J. Wu, *Angew. Chem. Int. Ed.* **2016**, *55*, 8615–8619; c) P. Hu, J. Wu, *Can. J. Chem.* **2017**, *95*, 223–233; d) Z. Sun, S. Lee, K. H. Park, X. Zhu, W. Zhang, B. Zheng, P. Hu, Z. Zeng, S. Das, Y. Li, *J. Am. Chem. Soc.* **2013**, *135*, 18229–18236.

[15] a) A. Konishi, Y. Hirao, K. Matsumoto, H. Kurata, R. Kishi, Y. Shigeta, M. Nakano, K. Tokunaga, K. Kamada, T. Kubo, *J. Am. Chem. Soc.* **2013**, *135*, 1430–1437; b) A. Konishi, Y. Hirao, H. Kurata, T. Kubo, M. Nakano, K. Kamada, *Pure Appl. Chem.* **2014**, *86*, 497–505.

[16] a) J. Casado, *Top. Curr. Chem.* **2017**, *375*, 209; b) Z. Zeng, M. Ishida, J. L. Zafra, X. Zhu, Y. M. Sung, N. Bao, R. D. Webster, B. S. Lee, R.-W. Li, W. Zeng, Y. Li, C. Chi, J. T. Lopez Navarrete, J. Ding, J. Casado, D. Kim, J. Wu, *J. Am. Chem. Soc.* **2013**, *135*, 6363–6371; c) Z. Zeng, J. Wu, *Chem. Rec.* **2015**, *15*, 322–328.

[17] a) T. Kubo, M. Sakamoto, M. Akabane, Y. Fujiwara, K. Yamamoto, M. Akita, K. Inoue, T. Takui, K. Nakasuji, *Angew. Chem. Int. Ed.* **2004**, *43*, 6474–6479; b) T. Kubo, A. Shimizu, M. Sakamoto, M. Uruichi, K. Yakushi, M. Nakano, D. Shiomi, K. Sato, T. Takui, Y. Morita, *Angew. Chem. Int. Ed.* **2005**, *44*, 6564–6568; c) A. Shimizu, Y. Hirao, K. Matsumoto, H. Kurata, T. Kubo, M. Uruichi, K. Yakushi, *Chem. Commun.* **2012**, *48*, 5629–5631; d) A. Shimizu, T. Kubo, M. Uruichi, K. Yakushi, M. Nakano, D. Shiomi, K. Sato, T. Takui, Y. Hirao, K. Matsumoto, *J. Am. Chem. Soc.* **2010**, *132*, 14421–14428.

[18] a) S. Dong, T. Y. Gopalakrishna, Y. Han, H. Phan, T. Tao, Y. Ni, G. Liu, C. Chi, *J. Am. Chem. Soc.* **2019**, *141*, 62–66; b) B. Purushothaman, M. Bruzek, S. R. Parkin, A. F. Miller, J. E. Anthony, *Angew. Chem. Int. Ed.* **2011**, *50*, 7013–7017; c) M. Bendikov, H. M. Duong, K. Starkey, K. Houk, E. A. Carter, F. Wudl, *J. Am. Chem. Soc.* **2004**, *126*, 7416–7417; d) S. N. Intorp, M. Hodecker, M. Müller, O. Tverskoy, M. Rosenkranz, E.

Dmitrieva, A. A. Popov, F. Rominger, J. Freudenberg, A. Dreuw, *Angew. Chem. Int. Ed.* **2020**, *59*, 12396–12401.

[19] a) A. Shimizu, R. Kishi, M. Nakano, D. Shiomi, K. Sato, T. Takui, I. Hisaki, M. Miyata, Y. Tobe, *Angew. Chem. Int. Ed.* **2013**, *52*, 6076–6079; b) J. J. Dressler, Z. Zhou, J. L. Marshall, R. Kishi, S. Takamuku, Z. Wei, S. N. Spisak, M. Nakano, M. A. Petrukhina, M. M. Haley, *Angew. Chem. Int. Ed.* **2017**, *56*, 15363–15367.

[20] a) J. J. Dressler, A. C. Valdivia, R. Kishi, G. E. Rudebusch, A. M. Ventura, B. E. Chastain, C. J. Gómez-García, L. N. Zakharov, M. Nakano, J. Casado, *Chem* **2020**, *6*, 1353–1368; b) J. E. Barker, J. J. Dressler, A. Cárdenas Valdivia, R. Kishi, E. T. Strand, L. N. Zakharov, S. N. MacMillan, C. J. Gómez-García, M. Nakano, J. Casado, *J. Am. Chem. Soc.* **2020**, *142*, 1548–1555; c) H. Miyoshi, M. Miki, S. Hirano, A. Shimizu, R. Kishi, K. Fukuda, D. Shiomi, K. Sato, T. Takui, I. Hisaki, *J. Org. Chem.* **2017**, *82*, 1380–1388; d) J. J. Dressler, M. Teraoka, G. L. Espejo, R. Kishi, S. Takamuku, C. J. Gómez-García, L. N. Zakharov, M. Nakano, J. Casado, M. M. Haley, *Nat. Chem.* **2018**, *10*, 1134–1140; e) G. E. Rudebusch, J. L. Zafra, K. Jorner, K. Fukuda, J. L. Marshall, I. Arrechea-Marcos, G. L. Espejo, R. Ponce Ortiz, C. J. Gomez-Garcia, L. N. Zakharov, *Nat. Chem.* **2016**, *8*, 753–759.

[21] a) D. Doehnert, J. Koutecky, *J. Am. Chem. Soc.* **1980**, *102*, 1789–1796; b) K. Yamaguchi, *Chem. Phys. Lett.* **1975**, *33*, 330.

[22] T. Moss, A. Greiner, *Adv. Mater. Interfaces* **2020**, *7*, 1901858.

[23] a) R. Heimann, J. Kleiman, N. Salansky, *Nature* **1983**, *306*, 164–167; b) M. Liu, V. I. Artyukhov, H. Lee, F. Xu, B. I. Yakobson, *ACS Nano* **2013**, *7*, 10075–10082.

[24] a) E. J. Bylaska, R. Kawai, J. H. Weare, *J. Chem. Phys.* **2000**, *113*, 6096–6106; b) T. Torelli, L. Mitas, *Phys. Rev. Lett.* **2000**, *85*, 1702.

[25] M. M. Hansmann, M. Melaimi, D. Munz, G. Bertrand, *J. Am. Chem. Soc.* **2018**, *140*, 2546–2554.

[26] A. A. Fokin, L. V. Chernish, P. A. Gunchenko, E. Y. Tikhonchuk, H. Hausmann, M. Serafin, J. E. P. Dahl, R. M. K. Carlson, P. R. Schreiner, *J. Am. Chem. Soc.* **2012**, *134*, 13641–13650.

[27] B. Cirera, A. Sánchez-Grande, B. de la Torre, J. Santos, S. Edalatmanesh, E. Rodríguez-Sánchez, K. Lauwaet, B. Mallada, R. Zbořil, R. Miranda, O. Gröning, P. Jelínek, N. Martín, D. Ecija, *Nat. Nanotechnol.* **2020**, *15*, 437–443.

[28] Deposition Numbers CCDC 2256975 (for (*o*-1)₂), 2256976 (for *p*-2), 2256977 (for *p*-1), 2256978 (for *p*-0) contain the supplementary crystallographic data for this paper. These data are provided free of charge by the joint Cambridge Crystallographic Data Centre and Fachinformationszentrum Karlsruhe Access Structures service.

[29] a) C. Seel, F. Vögtle, *Angew. Chem. Int. Ed. Engl.* **1992**, *31*, 528–549; b) G. J. Rowlands, *Org. Biomol. Chem.* **2008**, *6*, 1527–1534.

[30] T. Nishiuchi, D. Ishii, S. Aibara, H. Sato, T. Kubo, *Chem. Commun.* **2022**, *58*, 3306–3309.

[31] a) S. Medina Rivero, J. Urieta-Mora, A. Molina-Ontoria, C. Martín-Fuentes, J. I. Urgel, M. Zubiria-Ulacia, V. Lloveras, D. Casanova, J. I. Martínez, J. Veciana, *Angew. Chem. Int. Ed.* **2021**, *60*, 17887–17892; b) T. Takahashi, K.-i. Matsuoka, K. Takimiya, T. Otsubo, Y. Aso, *J. Am. Chem. Soc.* **2005**, *127*, 8928–8929.

[32] L. Moshniaha, M. Żyła-Karwowska, P. J. Chmielewski, T. Lis, J. Cybińska, E. Gońka, J. Oschwald, T. Drewello, S. M. Rivero, J. Casado, M. Stępień, *J. Am. Chem. Soc.* **2020**, *142*, 3626–3635.

[33] C. Bannwarth, S. Ehlert, S. Grimme, *J. Chem. Theory Comput.* **2019**, *15*, 1652–1671.
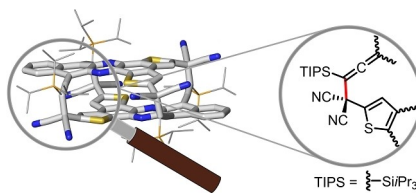
Research Articles

Diradicals

K. Fuchs, S. Medina Rivero, A. Weidlich,
F. Rominger, N. Israel, A. A. Popov,
A. Dreuw,* J. Freudenberg,* J. Casado,*
U. H. F. Bunz* —————— e202305712

Dimerization of a Reactive Azaacene Diradical: Synthesis of a Covalent Azaacene Cage

TIPS = $\text{Si}i\text{Pr}_3$

A head-to-tail dimerization of two reactive dicyanomethyl diradicals forms a covalent azaacene cage. In this cascade, four new, elongated σ-CC-bonds (marked in red) are formed and the internal alkynes transformed into cumulenes. The cage was investigated via several spectroscopy methods at different temperatures, suggesting the reformation of its constituting diradical.